

Optofluidic waveguides: I. Concepts and implementations

Holger Schmidt · Aaron R. Hawkins

Received: 1 March 2007 / Accepted: 27 June 2007 / Published online: 22 August 2007
© Springer-Verlag 2007

Abstract We review recent developments and current status of liquid-core optical waveguides in optofluidics with emphasis on suitability for creating fully planar optofluidic labs-on-a-chip. In this first of two contributions, we give an overview of the different waveguide types that are being considered for effectively combining micro and nanofluidics with integrated optics. The large number of approaches is separated into conventional index-guided waveguides and more recent implementations using wave interference. The underlying principle for waveguiding and the current status are described for each type. We then focus on reviewing recent work on microfabricated liquid-core antiresonant reflecting optical (ARROW) waveguides, including the development of intersecting 2D waveguide networks and optical fluorescence and Raman detection with planar beam geometry. Single molecule detection capability and addition of electrical control for electrokinetic manipulation and analysis of single bioparticles are demonstrated. The demonstrated performance of liquid-core ARROWs is representative of the potential of integrated waveguides for on-chip detection with ultrahigh sensitivity, and points the way towards the next generation of high-performance, low-cost and portable biomedical instruments.

Keywords Optofluidics · Integrated optics · Waveguides · Fluorescence spectroscopy · Single molecule detection

1 Introduction

Optofluidics is a relatively new field (Ehlert and Buettgenbach 1999) that has seen rapid development over the last few years. There are several reasons that have contributed to this trend. The combination of optics and fluidics is a very natural one as optical microscopy has been used for centuries in biology to study cells and other biological molecules and specimens that typically exist in aqueous solution. Similarly, other fields such as chemistry, toxicology, or environmental studies routinely use optical methods to analyze liquids and liquid solutions. The implementation of this natural connection in small chip-scale devices required the ability to control and manipulate small volumes of liquids reliably and rapidly. Consequently, the emergence of optofluidics was preceded by a large body of research work on micro and nanofluidics that has led to the miniaturization of fluidic control mechanisms such as valves and pumps and to the realization of numerous fluidic devices (Whitesides 2006; Squires and Quake 2005; Atencia and Beebe 2005; Ng et al. 2002). Finally, in the last couple of year the first optofluidic devices have been developed, showing two complementary points of view, the use of optical methods to study fluids, and the use of fluids to manipulate optical devices. Such devices include adaptive lenses (Zhang et al. 2003), optofluidic microscopes (Heng et al. 2006), fluidic dye lasers (Balslev and Kristensen 2005) and others. Especially promising applications are biosensing and biodetection devices. In particular, the small dimensions and fluid

H. Schmidt (✉)
School of Engineering, MS: SOE-2, UC Santa Cruz,
1156 High Street, Santa Cruz, CA 95064, USA
e-mail: hschmidt@soe.ucsc.edu

A. R. Hawkins
ECEn Department, Brigham Young University,
459 Clyde Building, Provo, UT 84602, USA

volumes typically present on a chip are ideally suited for carrying out single molecule detection (Craighead 2006). Single molecule detection is attractive for both fundamental research and biosensing applications, due to the ability to analyze molecules at the ultimate sensitivity limit, but has typically required bulky and costly microscopy setups (Moerner and Fromm 2003).

The growing interest in optofluidics has led to a series of recent comprehensive reviews that detail these developments (Psaltis et al. 2006; Monat et al. 2007; Craighead 2006). In these articles, general issues such as fabrication, light sources, applications, and system concepts are discussed. Our intent for this and the immediately following contribution is to provide a more focused review of the current state of the art of liquid-core waveguides (LCW) for optofluidic devices. The continuing thrust towards more compact and robust optofluidic labs-on-a-chip entails the integration of both fluidic and optical elements on the same chip. Waveguides are the key element of the optical structure, equivalent to the liquid channel on the fluidic side. Maximum integration and functionality will only be possible with large design flexibility and require the ability to use fluidic waveguides for guiding both light and liquid through the same physical volume. Concurrently with the developments in optofluidics, major progress in the field of hollow and liquid core waveguides was made that has only recently started to impact optofluidic platforms. This review presents a snapshot of the current state of this continuing process and is split into two parts. The basic principles of LCW and current optofluidic capabilities using these waveguides are discussed in the present contribution, while the following article (Optofluidic Waveguides: II. Fabrication and Structures) discusses fabrication approaches and challenges for creating these waveguides and integrating them into larger systems.

The remainder of this article is organized as follows. Section 2 contains a comprehensive overview of the different LCW used for integrated optofluidics, their physical operating principles, and current device implementations. Sections 3 and 4 focus on recent work done by our groups on liquid-core antiresonant reflecting optical (ARROW) waveguides which have been used to implement single molecule detection on a planar optofluidic chip. The article concludes with a summary in Sect. 5.

2 Waveguide types for planar optofluidics

2.1 Total internal reflection based

The overwhelming majority of optical waveguides traditionally used in solid state optoelectronics operates based on total internal reflection (TIR) (Coldren and Corzine

1995; Agrawal 2006). This concept—also referred to as index guiding, along with the terminology used throughout this article is illustrated in Fig. 1a. The figure depicts a side view of a generic slab waveguide based on index guiding where a high refractive index (n_c) core region is surrounded by low index (n_s) cladding materials. Light propagation occurs in the longitudinal (z) direction, and is illustrated by a representative light ray that is incident on the core-cladding interface at an angle θ above the critical angle for total internal reflection $\theta_c = \arcsin(n_s/n_c)$. Under these conditions, the light cannot propagate in the cladding material and the power remains confined to the waveguide core. Lossless propagation with propagation wave vector β is, in principle, possible if the total phase shift accumulated by the ray in transverse (y) direction equals a multiple of 2π (Yeh 2005). This mode condition as well as the spatial distribution of the electromagnetic field in the waveguide can also be derived by solving Maxwell's equations with the appropriate boundary conditions. The index guiding principle can be implemented in one and two dimensions and for arbitrary cross sections (Okamoto 2005). Most commonly used are cylindrical (optical fibers) and rectangular (ridge or buried) waveguide cross sections in the transverse (y) and lateral (x) directions.

The requirement for the refractive indices of core and cladding $n_c > n_s$ is easy to fulfill in solid-state devices, but

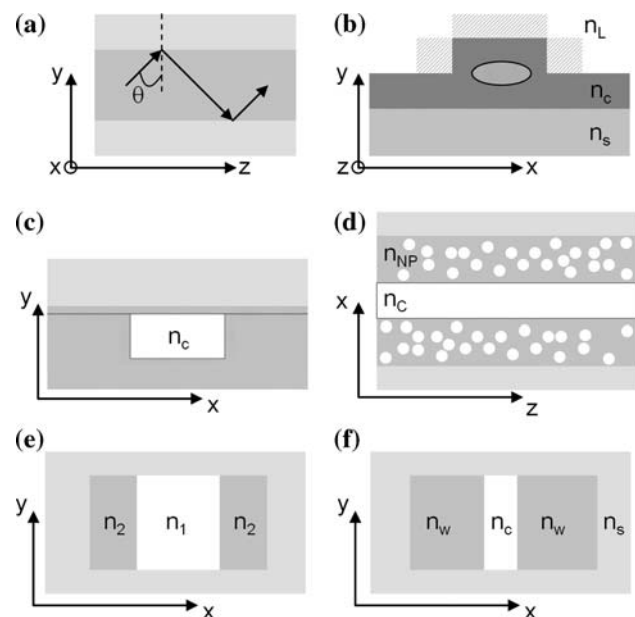


Fig. 1 Total internal reflection (TIR) based waveguides. **a** TIR principle in slab waveguide, **b** cross section of solid core ridge waveguide with mode area (ellipse) and penetration area into surrounding liquid (hatched areas); **c** liquid-core waveguide (LCW) cross section, **d** nanoporous cladding waveguide (side view), **e** liquid-liquid core (L^2) waveguide (cross section); **f** slot waveguide (cross section)

poses a severe problem for optofluidics as the index of water and most aqueous solutions is relatively low (~ 1.33) compared to that of the solid materials that have been used for microfluidic fabrication including both polymer and silicon based approaches (1.4–3.5). At first, this seems to preclude the use of index guiding for planar optofluidics, but several clever approaches have been developed to build TIR-based optofluidic devices. These are schematically shown in Fig. 1b–f and will be discussed individually.

2.1.1 Evanescent wave guiding

While the focus of this review is on liquid-core waveguides, i.e., the case where light and fluid are transported in the same volume, we include evanescent wave based devices because they represent the transition between all-solid-state and integrated optofluidic devices. Figure 1b shows the cross section of a typical implementation. Light is guided in a high index waveguide by TIR in the high-index ridge as illustrated by the elliptical mode in the center of the waveguide. While no far-field propagation can occur in the surrounding liquid (index n_L), the electric field decays exponentially outside the core. The intensity penetration depth q of this evanescent wave is given by (Yeh 2005)

$$q = \frac{1}{2} [\beta^2 - n_L^2 k_0^2]^{-1/2} \quad (1)$$

where k_0 is the vacuum wave vector. Typical penetration depths are on the order of 100–200 nm which means that an optical interaction between the waveguide and the liquid can take place at the interface. The available interaction area between waveguide and liquid is symbolized by the cross-hatched region in Fig. 1b. It can then be used for surface-sensitive molecular detection either by coupling light emitted from molecules within q into the waveguide or by exciting such molecules using the evanescent field propagating in the waveguide. Popular material systems are the silicon-on-insulator (SOI) system (Kurdi and Hall 1988; Soref et al. 1991a), polymers on silicon, or polymer-based waveguides, e.g., UV-exposed PMMA (Koo et al. 2003). Chemical and biological detection has successfully been demonstrated using this concept (Tiefenthaler and Lukosz 1989). While a simple waveguide analysis would predict very small sub-micron dimensions of the ridge to achieve single-mode propagation, it has been shown that these waveguides can in fact operate with a single mode for much larger dimensions as long as higher order modes have very high loss (Soref et al. 1991b). This allows for efficient interfacing with single mode optical fibers whose mode diameters are on the order of a few micrometers. If a large penetration depth in the liquid is desired, so-called reverse symmetry waveguides can be used. The electric

field penetrates more deeply in the cladding material with the higher refractive index which is usually the substrate. By using a suitable spacer layer such as a low-index mesoporous material (Horvath et al. 2002) or a thin metal layer (Zourob et al. 2003; White et al. 2007) at the bottom of the core, the field penetration into the liquid can be significantly enhanced. Evanescent field-based waveguides are well suited for study and detection of particles in immediate contact to the surface such as cells, but are limited for use with freely diffusing particles that need to be brought within the optical interaction volume. Other issues include the low efficiency of the light-particle interaction as most of the optical power is confined in the solid core. This limitation is overcome in the LCW that will be described in the remainder of this section.

2.1.2 Liquid-core waveguides

The most obvious approach to achieving index guiding in fluidic channels is to use a solid cladding material with a refractive index below 1.33. As discussed above, this task is not trivial, but there is a class of fluorinated polymers, such as Teflon AF that have been successfully used to build LCWs. Teflon AF has an index of 1.29 and has been incorporated as a cladding layer both in cylindrical tubes and on materials that were wafer-bonded to form a rectangular shaped hollow cross section (Schelle et al. 1999; Datta et al. 2003). The latter is illustrated in Fig. 1c where the cross-hatched areas represent the Teflon AF cladding which also forms the bonding interface. Low-loss light propagation in the liquid core and fluorescence detection of dye with nanomolar concentration (Datta et al. 2003) have been successfully demonstrated. To date, LCWs have been fabricated with large core diameters of 200–500 μm and Teflon AF cladding thicknesses on the order of a few μm with relatively large fluctuations. Single-mode waveguides are difficult to achieve because the core-cladding index difference of 0.04 results in required core thicknesses on the order of 1–2 μm and the Teflon AF thickness is difficult to control on this length scale.

2.1.3 Nanoporous cladding waveguides

Another way to form a low-index cladding material is to start with a high-index solid material and add air pores until the average index is low enough to facilitate waveguiding. This has the advantage that the cladding index can be tuned by varying the air fraction and that some of the adhesion problems that Teflon AF exhibits can potentially be overcome. Figure 1d shows a schematic image of a slab waveguide that has a nanoporous cladding with index

$n_{\text{NP}} < n_{\text{C}}$ embedded within a high index substrate. To date, nanoporous claddings have been implemented using a “sacrificial porogen” approach in which an organic phase is removed from a phase-separated polymer hybrid (Risk et al. 2004). Only 1D confinement in transverse (y) direction has been demonstrated using this method. However, the existence of low loss modes and the wide tuning range of the cladding index ($1.15 < n_{\text{NP}} < 1.37$) make this a very promising technology if a way to create a lateral nanoporous cladding for complete mode confinement can be developed.

2.1.4 Liquid–liquid core (L^2) waveguides

A clever way to circumvent the problem of finding a low-index solid cladding material is to use two different liquids with different refractive indices inside a larger fluidic channel. A cross section of such a liquid–liquid or L^2 waveguide is shown in Fig. 1e. As long as the index of the cladding liquid (index n_{S}) is smaller than that of the core liquid (index n_{I}) and the cladding layer is thicker than a few μm , index guiding in x -direction can be achieved. This concept was first demonstrated using CaCl_2 ($n_{\text{I}} = 1.445$) and water as core/cladding liquids, respectively, embedded in PDMS ($n = 1.4$) (Wolfe et al. 2004). The liquids were introduced into the channel through separate fluidic inlets and exhibited relatively slow mixing along the channel due to the laminar flow conditions. Both single and multi-mode operation were demonstrated although single-mode operation in the approximately 10 μm wide cores was only possible after the index contrast had been reduced by mixing along the channel to ~ 0.002 . The L^2 waveguide concept is perfectly suited for optofluidics as in this case control over the fluidic properties allows modification of the optical performance. This dynamic tuning ability is the biggest strength of the L^2 waveguide approach and several optofluidic functions have been demonstrated, including an optical switch (Wolfe et al. 2004), a fluorescent light source (Vezenov et al. 2005), optical splitters (Wolfe et al. 2005), and wavelength filters (Wolfe et al. 2005). Another inherent advantage of L^2 waveguides is that the propagation loss should be independent of the channel roughness (at least along the x -direction) although actual loss values of these waveguides have not been published yet. L^2 waveguides are likely limited by the susceptibility of the core-cladding interface to vibrations and diffusion effects, such as the change in index contrast due to core-cladding intermixing and the diffusion of analyte molecules of interest into the cladding regions. Aqueous core solutions ($n_{\text{I}} = 1.33$) could also pose a problem since one is then faced with the original refractive index problem in the transverse (y)

direction. This issue, however, can be addressed using hybrid approaches (see Sect. 2.2). Therefore, the tunability of L^2 waveguides is likely to provide functionality in future optofluidic devices, possibly integrated with solid core waveguides that can continue guiding the light after a short (mm-scale) L^2 section.

2.1.5 Slot waveguides

The waveguides discussed so far all feature core dimensions of ten to hundreds of micrometers. The recently proposed and demonstrated slot waveguide is an alternative in which index guiding can be realized in nanoscale cross sections, thereby providing an opportunity for extending waveguide based optofluidics into the nanofluidic regime (Almeida et al. 2004; Xu et al. 2004). The cross section of a slot waveguide as shown in Fig. 1f appears quite similar to that of the L^2 waveguide. Here, however, the core medium has the *lowest* index (n_{C}) in the structure. The immediately adjacent medium has the highest index (n_{W}) so that analytical mode solutions for this structure exist. The key for confining a substantial portion of the optical power in the low-index core medium is twofold. First, the width of the core has to be smaller than the penetration depth of the evanescent wave in the core medium, leading to nanoscale core dimensions on the order of 100 nm. Secondly, if x -polarized light is used, application of the electromagnetic boundary conditions at the $n_{\text{C}}/n_{\text{W}}$ interface results in a discontinuity of the electric field (TM mode). It can be easily shown that the electric field strength in the core is increased by a factor of $n_{\text{W}}^2/n_{\text{C}}^2$. As a result, up to 30% of the optical power can be confined in a 100 nm narrow core for a high index contrast system such as Si/air with a large enhancement factor of 12 (Almeida et al. 2004). This concept was experimentally demonstrated on an SOI platform with air as the core, silicon as cladding ($n_{\text{W}} = 3.5$), and SiO_2 ($n_{\text{H}} = 1.46$) as the encapsulating material (Xu et al. 2004). Efficient mode confinement, weak wavelength dependence and directional coupling were shown, but waveguide loss values have not been published yet. The small dimensions and high intensities available in a slot waveguide make this concept very attractive for optofluidic applications. Molecular interactions with the walls are likely to play a prominent role due to the large surface-to-volume ratio of the nanofluidic channels. Moreover, the field enhancement is somewhat reduced for aqueous cores [7 for a Si cladding, 1.2 for PDMS ($n = 1.45$)], but the very tight confinement and interaction area makes slot waveguides a prime candidate for optofluidic measurements at low analyte concentrations on a silicon platform.

2.2 Interference based

So far, we have seen that despite the initially discouraging index ratio between water and most solids, several waveguide types based on conventional index guiding have been developed that can be considered for planar optofluidics. A conceptually different approach to waveguiding is the use of wave interferences to localize the electromagnetic wave. In this case, the refractive index profile of the cladding is structured in the (x - y) cross section of the waveguide to create multiple reflections of the electric field that can interfere constructively or destructively. This notion is sketched in Fig. 2a where rays are shown to be incident on a structured dielectric medium (indices n_1 and n_2). As seen in the figure, the light is partially reflected at each interface. Only a few of the infinite number of reflected components are shown, and these have to be all added up to determine the total amount of reflected power. The key idea in the present context is that near-perfect reflection into the original medium can be achieved even if that medium has a lower index than all of the cladding layer materials. As in the case of index-guiding, several interference-based waveguide types have been developed that we will now describe individually.

2.2.1 Bragg fibers

A very important implementation of interference-based waveguiding is the special case where the dielectric cladding layers of Fig. 2a are repeated periodically and extend to infinity. The partial reflections are then equivalent to the Bragg reflections that are well known from X-ray analysis of crystalline materials. In complete analogy, the electric field propagating inside the periodic medium can be described by (Yeh et al. 1977)

$$E_K(x, z) = E_K(x) e^{iKx} e^{i\beta z} \tag{2}$$

where $E_K(x)$ is a periodic function with period Λ . The Bloch wave vector K reflects the periodicity of the structure (period Λ) and depends on Λ , the wave frequency ω , and the indices of the dielectric materials. Real (imaginary) values of K correspond to propagating (evanescent) solutions and lead to allowed (forbidden) regions, so-called bands, if K is plotted in an $\omega - \beta$ diagram. Due to the analogy with the behavior of electron waves in solid state materials, the periodic Bragg lattice is also called a 1D photonic crystal (PC). In order to utilize this periodic structure for integrated optofluidic waveguides, two conditions need to be fulfilled for the wavelength of interest. First, the Bragg lattice has to be highly reflective, i.e., one has to operate within a forbidden region of the K , and secondly, the transverse component of the wavevector has to fulfill the same phase resonance condition as in the case

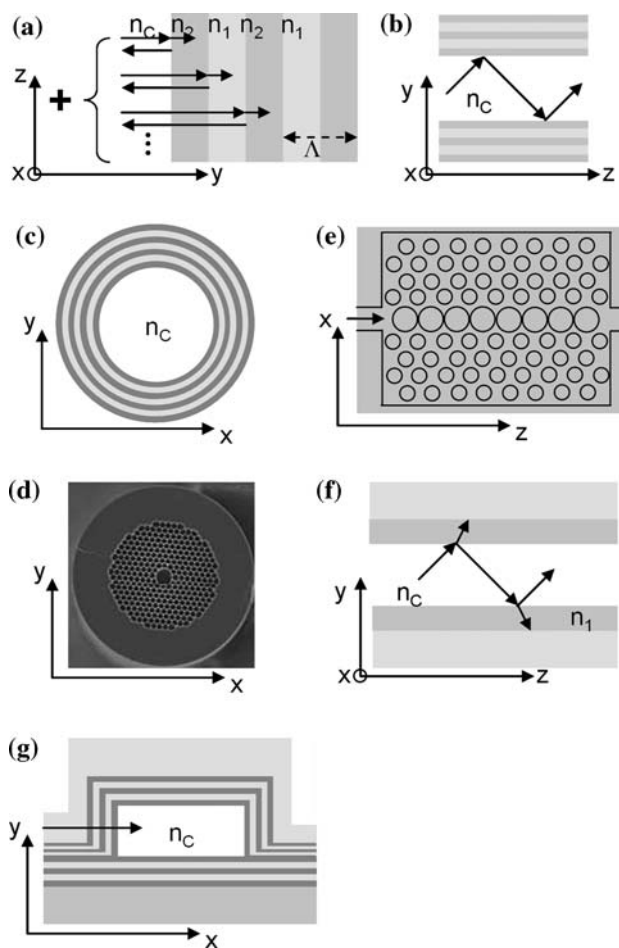


Fig. 2 Interference-based waveguides. **a** Schematic view of multiple interfering partial reflections from periodic dielectric multilayer stack (period Λ), **b** Bragg waveguide (side view), **c** Bragg fiber (cross section), **d** hollow-core photonic crystal fiber (HCPCF, cross section), **e** 2D planar photonic crystal (top view), **f** ARROW waveguide principle (side view), **g** liquid-core (LC) ARROW waveguide (cross section)

of index guiding to allow for transport of energy along the propagation (z) direction. If both conditions are fulfilled, the situation depicted in Fig. 2b emerges in which an incident ray is experiencing Bragg reflection from two periodic Bragg stacks and is guided along z . The similarity to Fig. 1a is evident, but the key difference is that now the core index n_c can be smaller than any of the refractive indices in the Bragg lattice. These Bragg slab waveguides were first proposed by Yeh and Yariv (1978), and a more comprehensive review including an analysis of the polarization dependence is given in (Yeh et al. 1977). The same general ideas can also be applied to 2D cylindrical cross sections that resemble conventional silica fibers. The cross section of such a Bragg fiber is shown in Fig. 2c and illustrates how the periodic layers surround a circular low index core resulting in an index profile that depends on the radial distance from the core center. The Bragg fiber was

first analyzed by Yeh et al. (1978) and later refined by Xu et al. (2000). The first experimental demonstrations of light guiding in an air-core Bragg fiber were given by Fink et al. (1999) using a large ~ 2 mm air core surrounded by alternating layers of tellurium and polymer, followed by 275 μm -core $\text{As}_2\text{Se}_3/\text{PES}$ -fibers for infrared guiding (Temelkuran et al. 2002). If the Bragg layers are designed to be reflective for all angles of incidence (omnidirectional guiding Winn et al. 1998), light can even propagate around bends with very low loss. This concept has been successfully developed into medical instruments for CO_2 laser delivery for otolaryngology and pulmonology (see <http://www.omni-guide.com>). Liquid-filled Bragg fibers have not been reported yet, but the concept is equally promising and applicable to aqueous core materials.

2.2.2 Hollow-core PC fiber

The PC concept is not restricted to 1D index periodicity. In fact, dielectric structures with 2D periodicity currently play a bigger role in waveguide-based optofluidics. Figure 2d shows the cross section of a hollow-core PC fiber (HC-PCF) (Cregan et al. 1999; Russell 2003). In this case, a hollow core with typical diameters between 5 and 20 μm is surrounded by a periodic arrangement of holes inside a silica network. As in the 1D case, the spatial structure of the air/silica index variation determines the propagation properties of the hollow fiber along the z -direction. HC-PCF-fiber can be used for optofluidic applications in two ways—by making either the hollow core or the surrounding holes the active fluidic interrogation volume. The latter approach has been taken to demonstrate surface-enhanced Raman detection in HC-PCF (Yan et al. 2006), and observing changes in the guiding properties of solid-core PCFs (Domachuk et al. 2004; Mach et al. 2002; Rindorf et al. 2006). Closer in the spirit of the present discussion are the recent demonstrations of light and particle guiding through the liquid-filled center core of a HC-PCF (Mandal and Erickson 2007) and the observation of fluorescence from HC-PCF whose central core holes were coated with fluorophores albeit without filling the cores with liquid (Smolka et al. 2007). Neither of the cylindrical fibers (1D-Bragg, 2D-HC-PCF) can be monolithically integrated on an optofluidic platform in a straightforward way. However, there should be opportunities to interface these types of waveguides with the remainder of the chip to create the desired functionalities.

2.2.3 2D PC-waveguides

The third approach to utilizing a photonic band gap structure for low-index waveguiding is schematically

depicted in Fig. 2e. Light propagation in the direction of the arrow is achieved by Bragg reflection (2D PC) in the x - z plane (Joannopoulos et al. 1995) and conventional index guiding in the third dimension. This concept was first realized using a central solid core silicon waveguide surrounded by periodic air holes to facilitate light guiding around tight bends (Loncar et al. 2000). A compelling feature of these PC-waveguides compared to their fiber counterparts is their planarity which is highly attractive for planar optofluidic integration. This direction has been pioneered at Caltech, mainly in the context of tuning the photonic properties of the waveguides by fluidic control. Specifically, nanofluidic tuning of the optical properties of a PC waveguide with the geometry of Fig. 2e was demonstrated (Erickson et al. 2006). By using multi-layer integration of the optical waveguide layer and a fluidic delivery layer, it was possible to address (fill) individual holes in the 2D PC-waveguide, in particular the central guiding row with the larger holes. The nanoscale spatial control and level of higher level integration in this platform is encouraging for future developments of fluidically controlled optics (McNab et al. 2003). 2D PC waveguides have not been used with liquid guiding channels. Conceptually, this should also be possible and would open up this approach to optical analysis of sample analytes in a LCW.

2.2.4 ARROW waveguides

The last type of interference-based waveguides that is being considered for optofluidics is antiresonant reflecting optical waveguides (ARROWs). ARROW waveguides are also based on an interference effect, but do not require the periodicity of a PC that results in the description of light propagation by means of Bloch wave vectors and allowed/forbidden bands. Consequently, a single dielectric layer is sufficient to provide low-loss propagation as illustrated in Fig. 2f. A light ray impinging from the low-index core on the high index ARROW layer (index n_1) is refracted into the ARROW layer due to the absence of total internal reflection. However, if the thickness of ARROW layer is chosen such that the round trip phase shift Φ_{RT} of the transverse (y) wave component in medium n_1 fulfills an antiresonance condition $\Phi_{\text{RT}} = m\pi$ (m odd), light is reflected back into the core with high efficiency and enables low loss light propagation in the low-index core. The required layer thickness t_1 is given by

$$t_1 = \frac{m\lambda}{4n_1} \left[1 - \frac{n_c^2}{n_1^2} + \frac{\lambda^2}{4n_1^2 d_c^2} \right]^{-0.5}; \quad m \text{ odd} \quad (3)$$

where d_c is the thickness of the core and λ the vacuum wavelength. The guiding efficiency of the ARROW

waveguide can be improved by adding more layers that fulfill the antiresonance condition. Unlike for PCs, these layers do not have to form a periodic stack which provides additional design flexibility. The ARROW concept was first implemented in solid-state waveguides to guide light through silicon dioxide on top of a silicon substrate using a silicon ARROW layer (Duguay et al. 1986). ARROWS were later used for semiconductor laser applications (Mawst et al. 1992; Patterson et al. 1999). The use of hollow-core ARROW waveguides was first demonstrated by Delonge and Fouckhardt (1995) who used alternating TiO_2 and SiO_2 ARROW layers to confine light in capillaries with $20 \times 20 \mu\text{m}^2$ cross section. More recently, liquid-core waveguides with ARROW confinement using silicon nitride (SiN) and silicon dioxide (SiO_2) have been demonstrated. They are very attractive for optofluidic applications due to the possibility of using silicon microfabrication technology. Both large multimode ($d_c > 100 \mu\text{m}$) (Bernini et al. 2004) and (quasi) single-mode ($d_c < 10 \mu\text{m}$) (Yin et al. 2004) ARROWS have been demonstrated using wafer bonding and sacrificial layer techniques, respectively. In both cases, the cross-sectional view of the waveguides typically appears as shown in Fig. 2g. The large-scale ARROWS can be interfaced with multimode fibers and have been used to demonstrate refractometric sensors (Campopiano et al. 2004) and flow cytometry (Bernini et al. 2007). These applications show that ARROWS can be used to represent both approaches to optofluidics, the use of fluids to change the optical properties of a device, and the use of optical methods to study fluids.

One essential property of ARROWS is that they can be designed to enable simultaneous guiding of light in a solid and a liquid-core waveguide. This property is desirable to enable the transfer of light in and out of fluidic channels to produce fully planar optofluidic architectures. This concept is illustrated by the arrow in Fig. 2g that enters the liquid core from a solid layer in which light is also confined by the ARROW mechanism. Intersecting waveguides were proposed by Schmidt et al. (2005) and their use for single molecules detection using planar beam geometry was demonstrated by Yin et al. (2006a). The use for single molecule detection along with the potential of further integration of functional elements such as wavelength filters and detectors make the liquid-core (LC) ARROW a prime candidate for future optofluidic detection on a chip.

2.3 Summary

In this section, we have reviewed current approaches to use planar waveguides in the context of optofluidics. Additional approaches such as hybrid L^2 /ARROW waveguides (Bernini et al. 2007), ARGOW waveguides (Schmidt et al.

2006), or even non-guiding zero-mode waveguide structures for single molecule detection (Levene et al. 2003) illustrate the large amount of activity in this field. In the remainder of this article, we will focus on liquid-core ARROW waveguides recently developed in our groups and their use for ultrahigh sensitivity detection.

3 Liquid-core ARROW waveguides

3.1 Theory

Before describing the experimental progress that has been made with LC-ARROWS over recent years, we first highlight a few theoretical aspects that are most relevant for designing functional optofluidic devices.

As with all waveguides, understanding and minimization of the waveguide loss is essential for good performance of the LC-ARROWS. The total loss of the rectangular structure shown in Fig. 2g can be approximated very well by considering two 1D problems along x and y and adding the 1D loss values (Marcatili's method 1969). This allows for quick loss calculations using standard transfer matrix methods (Yeh 2005) or the application of approximate expressions for 1D-loss in ARROW waveguides (Archambault et al. 1993). Horizontally (x) polarized light, for example, can be viewed as having TM polarization along x , and TE polarization along y . In the highly polarization-sensitive ARROW waveguide, the TM loss dominates. Therefore, the core should be wider in the lateral (x) direction to minimize this contribution (Yin et al. 2004). Other strategies for loss minimization by optimizing the index contrast for maximum reflection per layer have been devised (Uranus et al. 2006) but neglect the key influence of the reflection from the interface between the liquid core and the first cladding layer.

In Sect. 2, we have already alluded to the fact that coupling light into and out of liquid-core waveguides will be a key requirement for planar optofluidic architectures. In order to get a feeling for the requirements for LC-ARROW structures, it is instructive to consider the photonic band structure for the case of an infinite number of our commonly used silicon nitride/silicon dioxide layers. This analysis is not strictly valid for nonperiodic ARROW structures, e.g., if the bottom confinement layer design differs from the top, but illustrates the general ideas. Figure 3 shows the photonic dispersion diagram of frequency versus k -vector along the z -direction in the liquid-core channel. Light and dark regions correspond to evanescent and propagating waves, respectively. The diagonal white lines are the light lines in an aqueous core medium ($n_c = 1.33$), and the dash-dotted line indicates the design (vacuum) wavelength (here 690 nm). Right and left halves

of the diagram correspond to TE and TM waves, respectively. If designed correctly, light propagates with high reflectivity from the ARROW layers along the z -direction with near-grazing incidence, falling within a light (green) colored forbidden band for both TE and TM polarization near the light line as indicated by the two dashed arrows. At the same time, the ARROW layers create an allowed band [dark (blue) color] and are highly transmissive at near-normal incidence ($\beta = 0$) (solid white arrow). They are, therefore, not omnireflecting in a planar optofluidic device. Indeed, the high transmission at normal incidence is necessary to ensure efficient coupling into and out of the liquid core.

From a practical standpoint, relatively simple guidelines to design the top ARROW layers for efficient performance have been derived (Schmidt et al. 2005). A typical fluorescence experiment requires low-loss propagation of the excitation signal at wavelength λ_{exc} in the solid-core waveguide its efficient transmission into and out of the liquid core [condition $t_1 = l\lambda_{\text{exc}}/(2n_1)$; $l = \text{integer}$], and low-loss propagation of the fluorescence signal at λ_F along the liquid core [Eq. (3)]. The strategy to achieve this is to first optimize the thickness of the first cladding layer t_1 to fulfill both conditions, i.e., pick suitable integers l and m . The thickness of the second cladding material, t_2 , has no effect on the transmission problem. It can then be selected according to Eq. (3) to minimize the loss at λ_2 in the liquid core.

After optimizing the top layers for 2D waveguide arrays, the bottom ARROW layers can be tailored independently for additional functionality, e.g., for wavelength filtering. This effective decoupling of different design goals greatly

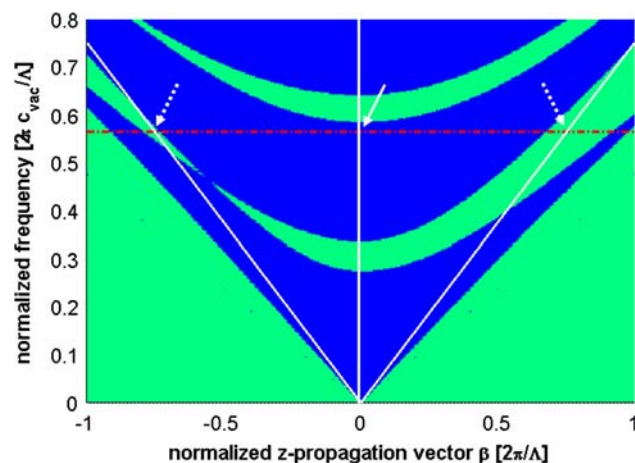


Fig. 3 Dispersion relation for LC-ARROW for TE (right half) and TM (left half) waves. Dark areas propagation forbidden (band gaps), light areas: propagation allowed; white solid lines: light lines; horizontal dash-dotted line: design wavelength (690 nm); dashed arrows: fundamental mode propagation along liquid core; solid arrow: reflection at normal incidence

enhances the versatility of the integrated ARROW approach. The application of ARROW design to integrated wavelength filtering has been illustrated with the example of Fluorescence Resonance Energy Transfer (FRET) (Strayer 1978) which involves one excitation and two emission (donor and acceptor) wavelengths. The bottom ARROW layers can be designed to filter out the excitation beam (high loss at λ_{exc}) while transmitting both donor and acceptor fluorescence (low loss at λ_{F1} and λ_{F2}) along the liquid core. These conditions in Eq. (3) result in an order triplet (m_{F1} , m_{F2} , m_{exc}) governed by,

$$m_{\text{exc}} = \frac{\lambda_{F2}}{\lambda_{\text{exc}}} m_{F2} \quad (4)$$

$$m_{F1} = \frac{\lambda_{F2}}{\lambda_{F1}} m_{F2} \quad (5)$$

Fig. 4 shows the calculated fundamental mode loss for a structure that was optimized as a filter for the common FRET dye pair Alexa 546/647 ($\lambda_{F1} = 580$ nm, $\lambda_{F2} = 668$ nm, $\lambda_{\text{exc}} = 546$ nm) (Hakanson et al. 2007). It is clearly seen that the design requirements for low and high loss regions are fulfilled and that the LC-ARROW dispersion can be tailored to a specific application, demonstrating the versatility of this platform.

3.2 Optical performance

Different versions of quasi single-mode LC-ARROWS have been fabricated. These are shown in Fig. 5 where a cross-sectional image of each waveguide type is shown along with an experimentally measured mode image of

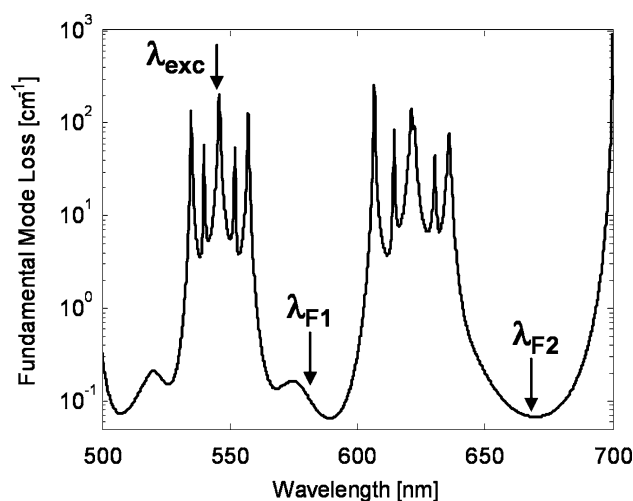


Fig. 4 LC-ARROW loss versus wavelength for FRET filter design featuring high loss at donor excitation wavelength and low loss at donor and acceptor emission wavelengths

light transmission through the core that confirms the interference-based light confinement. Figure 5a depicts an LC-ARROW with rectangular core and silicon nitride/oxide cladding layers (Yin et al. 2004). This design was used for all experiments described in Sect. 4 and corresponds to the schematic in Fig. 2g. Propagation losses well below 1/cm have been demonstrated in these structures (Yin et al. 2005b). Hollow-core ARROWs with pre-etched substrates (Fig. 5b) help reduce the TM loss in x -direction and are especially beneficial if the core material is air (Yin et al. 2005a). Arched-core ARROWs (Fig. 5c), finally, have several desirable mechanical properties and somewhat lower loss than their rectangular counterparts for the same mode area. The lowest LC-ARROW loss of 0.26/cm was measured using such a core (Yin et al. 2005b). More details regarding the fabrication and differences between these ARROW-types can be found in the following article Optofluidic Waveguides: II. Fabrication and Structures.

4 Fluorescence spectroscopy with planar LC-ARROWs

Light guiding in liquid core ARROW waveguides with quasi single-mode behavior was first demonstrated in 2004 (Yin et al. 2004) using ethylene glycol as the liquid core material and waveguide lengths ranging from ~ 1 mm to

~ 1 cm. A waveguide loss of 2.4/cm for a waveguide with a core cross section of $3.5 \times 24 \mu\text{m}$ was observed along with a strong wavelength dependence of the loss. After this initial demonstration of a planar optofluidic waveguide, the approach was continuously refined towards high sensitivity molecular detection on a chip.

4.1 Fluorescence and Raman scattering in linear waveguides

The first step in this direction is to show that the ARROW channels can be filled with a solution containing analyte molecules, and that a molecule-specific response can be generated and detected optically. Generation of optical signals from molecules in linear, open-ended LC-ARROWs was demonstrated for both fluorescence (Yin et al. 2004) and surface-enhanced Raman scattering (SERS) detection (Measor et al. 2007). Figure 6a shows the experimental situation for the fluorescence experiment (Yin et al. 2004) in top-down view. Due to the lack of fluidic control, open-ended channels are filled by capillary action with a solution of Alexa 647 dye molecules in ethylene glycol. Fluorescence is then generated by sending light from a HeNe laser (~ 1 mW) through a single mode fiber end-coupled to the ARROW facet. The generated signal is shown as a dashed arrow in this and all following figures. Here, fluorescence is detected at the other end of the channel after the copropagating excitation beam is filtered out. Figure 6b shows the fluorescence power as a function of dye concentration, indicating a concentration sensitivity of ~ 10 pM or ~ 500 molecules inside the excitation volume of 57 pl. In addition, a collection efficiency of $\sim 15\%$ of the emitted fluorescence signal for each facet could be extracted in good agreement with a theoretical model.

More recently, we investigated the possibility of Raman detection on an optofluidic chip (Measor et al. 2007). Raman detection is a very attractive detection mechanism because it is label-free and the inelastic scattering process results in molecule-specific spectral signatures. The inherently low Raman scattering efficiency is compensated by attaching the sample molecules to metallic nanoparticles that provide surface enhancement of the signal (SERS). The waveguide arrangement for the SERS measurements is shown in Fig. 7a. In this case, the liquid-core ARROW has an L-shape, i.e., one end is open, and the other is connected to a fluidic reservoir that is attached on the top of the chip and used to fill the channel with analyte solution. Excitation light is coupled into the liquid core via a solid core ARROW waveguide (SiO_2 core material) as described in Sect. 3, thereby demonstrating the concept of facilitating a transition between optofluidic and conventional solid-state waveguides. Here, SERS from rhodamine 6G (R6G)

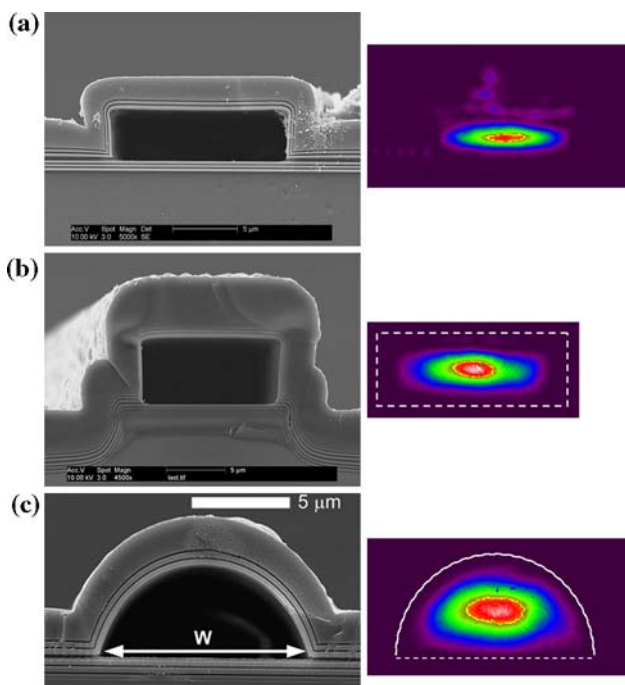


Fig. 5 Scanning electron microscope (*left*) and mode (*right*) images of LC-ARROW waveguides. **a** Rectangular core (Yin et al. 2004), **b** pre-etched substrate (Yin et al. 2005a), **c** arch-shaped core (Yin et al. 2005b)

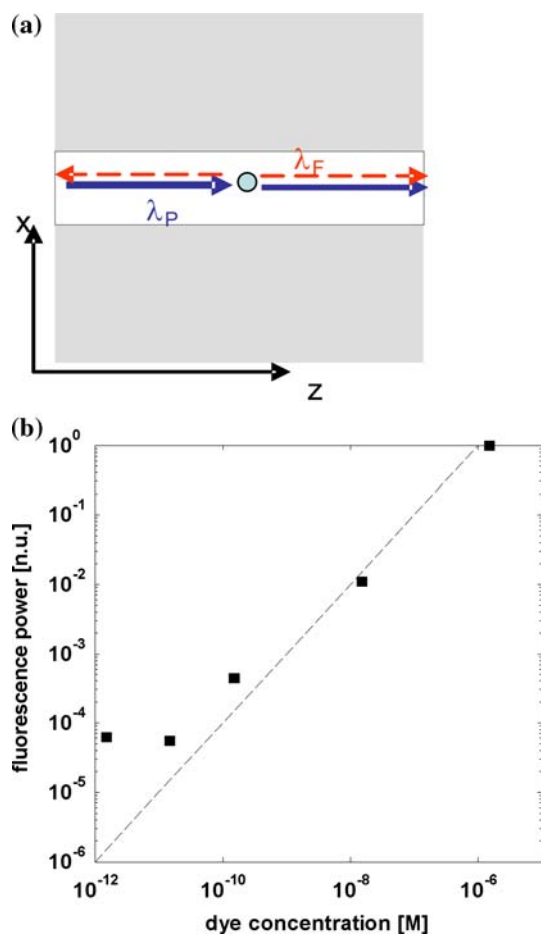


Fig. 6 Fluorescence detection in linear, open-ended LC-ARROWS. **a** Experimental beam geometry of molecular excitation (*top view* λ_P : excitation beam, λ_F : fluorescence signal); **b** detected fluorescence power versus Alexa 647 dye concentration (*symbols* data, *dashed line* linear fit)

molecules bound to silver nanoparticles was detected as a function of concentration and excitation power. The concentration dependence is shown in Fig. 7b along with the observed characteristic Raman spectrum of R6G. A detection sensitivity of 30 nM of freely diffusing R6G molecules demonstrated highly sensitive Raman detection on an optofluidic chip with planar optical beam paths.

4.2 Single molecule fluorescence

Conceptually, the next essential step is the realization of 2D waveguide structures following the design principles of Sect. 4.1 for excitation transmission into and fluorescence guiding along the liquid core. The sample geometry for this demonstration is sketched in Fig. 8a. As in the first fluorescence experiment, Alexa 647 dye molecules in ethylene glycol were used to fill the open-ended channel. Now, however, the fluorescence signal is excited with a beam

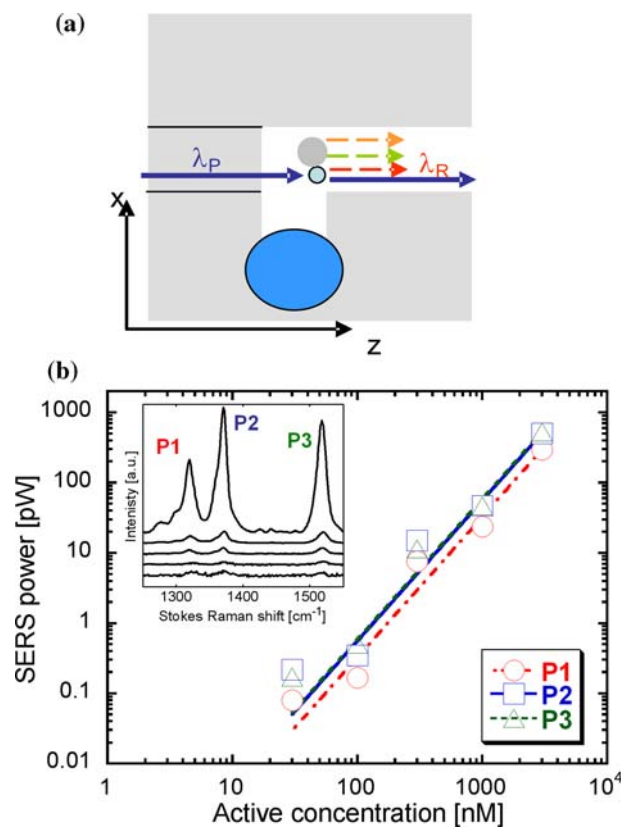


Fig. 7 SERS detection in open-ended LC-ARROW with fluidic reservoir. **a** Experimental beam geometry of excitation of rhodamine 6G molecules bound to silver nanoparticles (*top view* λ_P : excitation beam, λ_R : Raman signals); **b** R6G concentration-dependent SERS intensities for three representative Raman peaks *P1–P3*, *inset* spectra at various excitation powers

that intersects the liquid core perpendicularly. This has two highly beneficial effects. First, the excitation and fluorescence beam paths are spatially separated, leading to a substantial reduction in the number of background counts on the detector. Secondly, the excitation volume is now lithographically confined on the micron-scale in all three dimensions by the LC-ARROW cross section and the solid core waveguide width. This results in a sub-picoliter optical excitation volume of 85fl that is symbolized by the ellipse in Fig. 8a and is sufficiently small to enable single molecule fluorescence detection (Yin et al. 2006a). Figure 8b shows the detected fluorescence signal as a function of the number of molecules in the excitation volume. It can be seen that we can clearly distinguish single molecules on this chip without the need for expensive microscopy techniques. It was also demonstrated that fluorescence can be excited at different points along the liquid channel using four solid-core waveguides in parallel (Yin et al. 2006a), which suggests that 2D networks of liquid and solid-core waveguides are feasible.

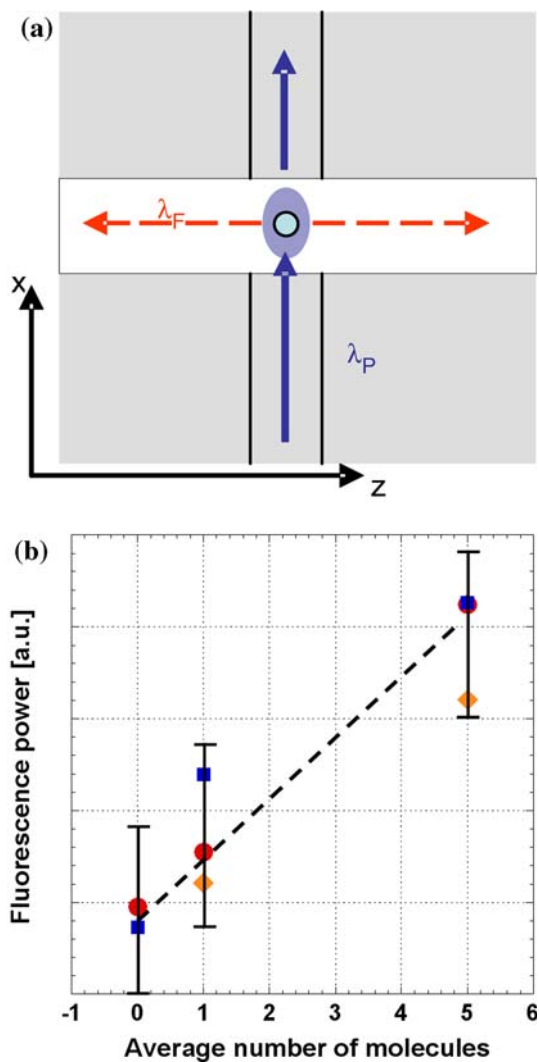


Fig. 8 Single molecule fluorescence detection in open-ended LC-ARROW intersection. **a** Experimental beam geometry of dye molecule in sub-picometer excitation volume (*gray ellipse*) (*top view* λ_p : excitation beam, λ_F : fluorescence signal); **b** fluorescence signal as function of molecules in excitation volume; *symbols* different experimental runs, *dashed line* linear fit

4.3 Electrically controlled fluorescence

In addition to providing the necessary optical infrastructure and sensitivity, any optofluidic device should also provide fluidic control, in particular methods to introduce liquid sample material into the channel and subsequently move it to the optical detection volume. To this end, we expanded the chip architecture as shown in Fig. 9a. In this device geometry, an S-shaped LC-ARROW is terminated by two fluidic reservoirs that are attached to the sample surface. The reservoirs serve the dual purpose of providing easy introduction and modification of the sample material as well as enabling the application of an electric field across the channel by placing electrodes inside the reservoirs.

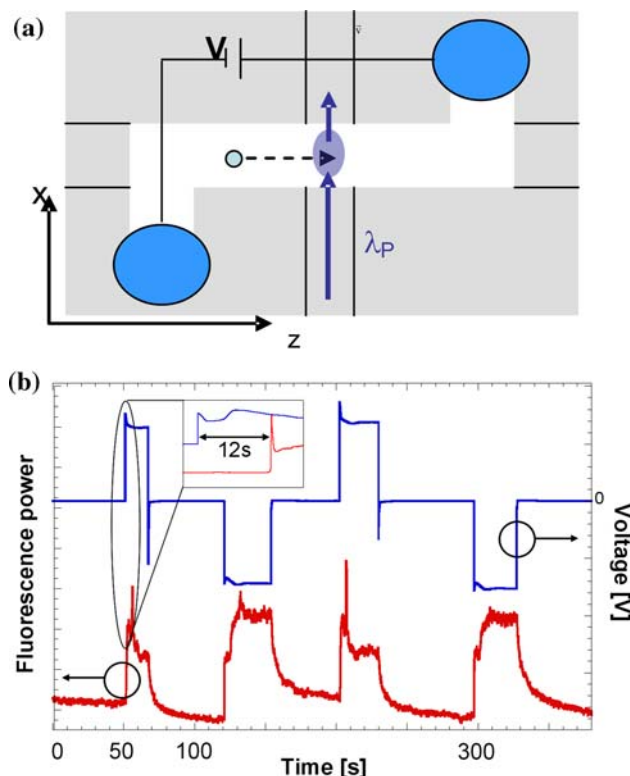


Fig. 9 Electrically controlled fluorescence detection in LC-ARROW optofluidic chip. **a** Experimental beam geometry of dye molecule moving in electric field towards optical excitation volume (*gray ellipse*) (*top view* λ_p : excitation beam); **b** applied voltage (*top*) and detected fluorescence signal (*bottom*) as function of time, *inset* details of initial time period showing delay between electrical and optical signal

Fluorescence is still captured and guided along the LC-ARROW as in Fig. 8a. However, now all optical beam paths (excitation and signal collection) are eventually terminated by solid-core waveguides that ensure fully planar beam geometry and a suitable interface to the edge of the chip or possibly other fluidic channels. The first demonstration of this concept is shown in Fig. 9b where both an applied voltage (*top*) and the detected fluorescence signal from Alexa 647 dye are plotted as a function of time (Yin et al. 2006b). The channel was initially filled with water followed by adding Alexa dye to one reservoir. When a voltage is applied, an optical signal is detected due to the electrokinetic movement of dye molecules into the waveguide intersection where the optical excitation takes place. The figure shows how the molecules are driven back and forth through the interaction volume as the polarity of the applied field alternates. The inset shows a magnified view of the initial signal and displays a 12 s delay between the application of the electric field and the onset of fluorescence detection. This delay corresponds to the time it takes the dye molecules to move from the reservoir to the optical excitation volume and allows us to deduce a dye velocity of

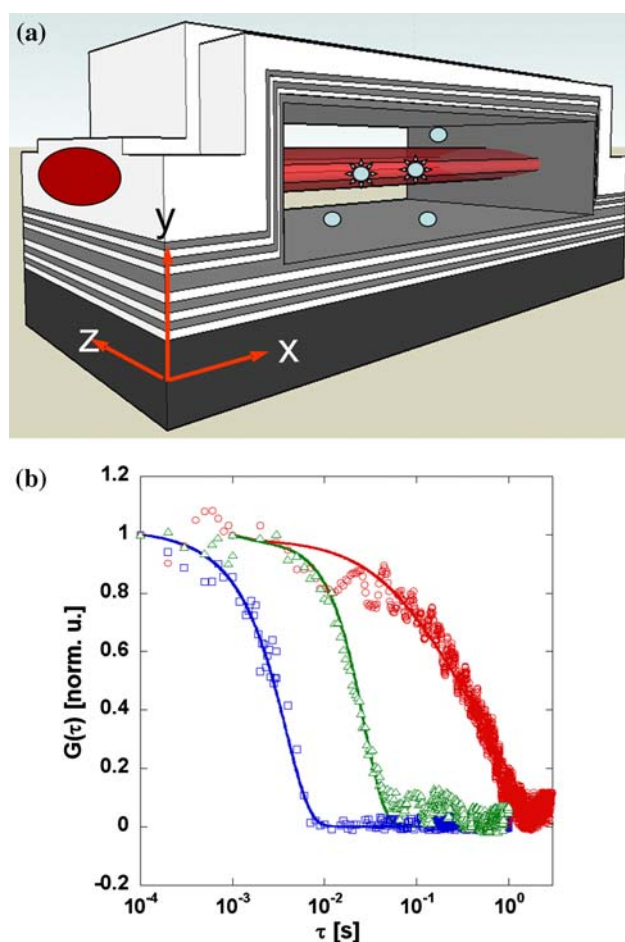


Fig. 10 Fluorescence correlation spectroscopy (FCS) of single biological nanoparticles in LC-ARROW optofluidic chip. **a** 3D view of optical excitation in waveguide intersection showing excited and non-excited molecules; **b** normalized FCS correlation signal versus time delay, from left to right Alexa 647 dye molecules (squares), labeled liposomes under 180 V bias (triangles), labeled liposomes without bias (circles); lines theory

0.28 mm/s. This initial experiment shows that it is possible to combine planar ARROW waveguide detection with electrical and simple microfluidic control.

4.4 Fluorescence correlation spectroscopy of single biological nanoparticles

After having shown optical, fluidic, and electrical access in the LC-ARROW chip, we used the setup shown in Fig. 9a to implement fluorescence correlation spectroscopy (FCS) with single particle resolution in this integrated setting. FCS is an advanced spectroscopy method that requires exquisite sensitivity, but is capable of resolving dynamic processes on the single molecule level (Rigler and Elson 2001). It is used, for example, to detect binding, cell structure, conformational changes, and in high-throughput

drug screening. Its versatility makes it an excellent choice for evaluating the analytical capabilities afforded by the planar optofluidic device. FCS is based on analyzing the fluctuations of the fluorescence signal, typically by computing its autocorrelation function $G(\tau)$. Figure 10a illustrates this idea by depicting a close-up view of the optical excitation volume at the waveguide intersection. In the figure, two molecules are within the excitation volume and fluoresce. As long as these two molecules remain inside this volume, the fluorescence fluctuations are highly correlated. Once any of these molecules diffuses out of this volume and is replaced by one that is initially outside, the correlation will be lost despite the fact that the total intensity is unchanged. Figure 10b shows three FCS auto-correlation curves measured on the LC-ARROW chip that illustrate the power of this technique. The general shape (large correlation for short delay times, small correlation at long times) is the same for all curves, but the details reveal the differences between the experiments. The leftmost curve was taken for Alexa 647 dye molecules and has the fastest rollover which is determined by the residence time of the sample molecule in the excitation volume. The extremely light dye molecules diffuse very fast so that the correlation is lost quickly. The other two curves are taken for larger biological nanoparticles, 200 nm diameter liposomes (lipid bilayer vesicles) filled with Alexa dye. Even though the dye fluorescence is detected, the resulting FCS curves represent the properties of the much larger and heavier liposomes. The difference between the liposome curves is the applied voltage between the reservoirs (0 and 180 V) which results in either diffusive or drift motion through the excitation volume and therefore different residence times. All three curves are matched very well by a theoretical model that was developed for the microphotonic environment of the LC-ARROW (Yin et al. 2007a). From the fits, we were able to extract the diffusion coefficients of the dye and liposomes (250 and $3 \mu\text{m}^2/\text{s}$, respectively) as well as the drift velocities of the liposome at 180 V (0.36 mm/s). In addition, the number of particles in the excitation volume N_p can be determined from the unnormalized traces (not shown) as $N_p = 1/G(0)$ (Rigler and Elson 2001) which yields $N_p(\text{dye}) = 0.36$ and $N_p(\text{liposome}) = 0.6$, respectively. These measurements demonstrate that the optofluidic LC-ARROW platform can be used to detect, analyze, and manipulate molecules and biological particles with single molecule sensitivity (Yin et al. 2007b).

5 Conclusions

The field of waveguide-based planar optofluidics is still in its early stages. Many of the hallmarks of integrated optics

such as predefined beam alignment, planar architecture, or compact device size provide strong incentives to replace bulky and expensive microscopes for applications that do not require imaging such as molecule detection and identification. In this review, we have seen that numerous promising approaches to implementing planar optical waveguide architectures exist, and none of them have been used to their full potential. It is likely that a key requirement for optical planarity will be the efficient transition of light from liquid to solid core waveguides for further processing and distribution on the chip. Therefore, one main criterion aside from the inherent waveguide properties for evaluating these methods will be to assess how they can be incorporated into a larger, multi-functional optofluidic system. Liquid-core ARROW waveguides have already been used for optofluidic measurements on the single molecule level on a planar chip, and other waveguide types have the potential to achieve both similar performance and to enable new functionalities. Facilitating this transition will continue to provide stimulation and challenges for innovative research in the years to come.

Acknowledgments We gratefully acknowledge the contributions of our colleagues D.W. Deamer, H.F. Noller, J.Z. Zhang, U. Hakanson, and students D. Yin, J.P. Barber, P. Measor, E. Lunt, M. Rudenko, and S. Kuehn. We also acknowledge funding for this work by the National Institutes of Health (NIH/NIBIB) under grants R21EB003430 and R01EB006097, the National Science Foundation (NSF) under grant ECS-0528730, a NASA/UARC Aligned Research Program (ARP) grant, a California Systemwide Biotechnology Research and Education Program Training Grant (UC-GREAT 2005-245), a National Academies Keck Futures Initiative Award (NAKFI-Nano14), and a grant from the David Huber Foundation.

References

- Agrawal G (2006) *Nonlinear fiber optics*, 4th edn. Academic, London
- Almeida VR, Xu Q, Barrios CA, Lipsen M (2004) Guiding and confining light in void nanostructures. *Opt Lett* 29:1209–1211
- Archambault JL, Black RJ, Lacroix S, Bures J (1993) Loss calculations for antiresonant waveguides. *J Lightwave Technol* 11:416–423
- Atencia J, Beebe DJ (2005) Controlled microfluidic interfaces. *Nature* 437:648–655
- Balslev S, Kristensen A (2005) Microfluidic single-mode laser using high-order Bragg grating and antiguiding segments. *Opt Exp* 13:344–351
- Bernini R, Campopiano S, Zeni L, Sarro PM (2004) ARROW optical waveguides based sensors. *Sens Actuators B* 100:143–146
- Bernini R, DeNuccio E, Minardo A, Zeni L, Sarro PM (2007) Integrated silicon optical sensors based on hollow core waveguide. *Proc SPIE* 6477:647714
- Campopiano S, Bernini R, Zeni L, Sarro PM (2004) Microfluidic sensor based on integrated optical hollow waveguides. *Opt Lett* 29:1894–1896
- Coldren LA, Corzine SW (1995) *Diode lasers and photonic integrated circuits*. Wiley, London
- Craighead H (2006) Future lab-on-a-chip technologies for interrogating individual molecules. *Nature* 442:387–393
- Cregan RF, Mangan BJ, Knight JC, Birks TA, Russell PSJ, Roberts PJ, Allan DC (1999) Single-mode photonic band gap guidance of light in air. *Science* 285:1537–1539
- Datta A, Eom I, Dhar A, Kuban P, Manor R, Ahmad I, Gangopadhyay S, Dallas T, Holtz M, Temkin H, Dasgupta P (2003) Microfabrication and characterization of teflon AF-coated liquid core waveguide channels in silicon. *IEEE Sens J* 3:788–795
- Delonge T, Fouckhardt H (1995) Integrated optical detection cell based on Bragg reflecting waveguides. *J Chromat A* 716:135–139
- Domachuk P, Nguyen HC, Eggleton BJ, Straub M, Gu M (2004) Microfluidic tunable photonic band-gap device. *Appl Phys Lett* 84:1838–1840
- Duguay MA, Kokubun Y, Koch T, Pfeiffer L (1986) Antiresonant reflecting optical waveguides in SiO₂-Si multilayer structures. *Appl Phys Lett* 49:13–15
- Ehlert A, Buettgenbach S (1999) Automatic sensor system for groundwater monitoring network. *Proc SPIE* 3857:61–69
- Erickson D, Rockwood T, Emery T, Scherer A, Psaltis D (2006) Nanofluidic tuning of photonic crystal circuits. *Opt Lett* 31:59–61
- Fink Y, Ripin DJ, Fan S, Chen C, Joannopoulos JD, Thomas EL (1999) Guiding optical light in air using an all-dielectric structure. *J Lightwave Technol* 17:2039–2041
- Hakanson U, Measor P, Yin D, Lunt E, Hawkins AR, Sandoghdar V, Schmidt H (2007) Tailoring the transmission of liquid-core waveguides for wavelength filtering on a chip. *Proc SPIE* 6477:647715
- Heng X, Erickson D, Baugh LR, Yaqoob Z, Sternberg PW, Psaltis D, Yang C (2006) Optofluidic microscopy: a method for implementing high resolution optical microscope on a chip. *Lab Chip* 6:1274–1276
- Horvath R, Lindvold LR, Larsen NB (2002) Reverse-symmetry waveguides: theory and fabrication. *Appl Phys B* 74:383–393
- Joannopoulos JD, Meade RD, Winn JN (1995) *Photonic crystals: molding the flow of light*. Princeton University Press, New Jersey
- Koo JS, Williams RB, Gawith CBE, Watts SP, Emmerson GD, Albanis V, Smith PGR, Grossel MC (2003) UV written waveguide devices using crosslinkable PMMA-based copolymers. *Electron Lett* 39:394–395
- Kurdi BN, Hall DG (1988) Optical waveguides in oxygen-implanted buried-oxide SOI structures. *Opt Lett* 13:175–177
- Levene MJ, Korlach J, Turner SW, Fouquet M, Craighead HG, Webb WW (2003) Zero-mode waveguides for single-molecule analysis at high concentrations. *Science* 299:682–686
- Loncar M, Nedeljkovic D, Doll T, Vuckovic J, Scherer A, Pearsall TP (2000) Waveguiding in planar photonic crystals. *Appl Phys Lett* 77:1937–1939
- Mach P, Dolinski M, Baldwin KW, Rogers JA, Kerbage C, Windeler RS, Eggleton BJ (2002) Tunable microfluidic optical fiber. *Appl Phys Lett* 80:4294–4296
- Mandal S, Erickson D (2007) Optofluidic transport in liquid core waveguiding structures. *Appl Phys Lett* 90:184103
- Marcatili EAJ (1969) Dielectric rectangular waveguide and directional coupler for integrated optics. *Bell Syst Technol J* 48:2071–2102
- Mawst LJ, Botez D, Zmudzinski C, Tu C (1992) Design optimization of ARROW-type diode lasers. *IEEE Phot Technol Lett* 4:1204–1206
- McNab S, Moll N, Vlasov Y (2003) Ultra-low loss photonic integrated circuit with membrane-type photonic crystal waveguides. *Opt Exp* 11:2927–2939
- Measor P, Lunt EJ, Seballos L, Yin D, Zhang JZ, Hawkins AR, Schmidt H (2007) On-chip surface-enhanced Raman scattering (SERS) detection using integrated liquid-core waveguides. *Appl Phys Lett* 90:211107

- Moerner WE, Fromm DP (2003) Methods of single-molecule fluorescence spectroscopy and microscopy. *Rev Sci Instr* 74:3597
- Monat C, Domachuk P, Eggleton BJ (2007) Integrated optofluidics: a new river of light. *Nat Photonics* 1:106–114
- Ng JMK, Gitlin I, Stroock AD, Whitesides GM (2002) Components for integrated PDMS microfluidic systems. *Electrophoresis* 23:3461–3473
- Okamoto K (2005) *Fundamentals of optical waveguides*, 2nd edn. Academic, London
- Patterson SG, Petrich SG, Ram RJ, Kolodziejski (1999) Continuous-wave room temperature operation of bipolar cascade laser. *Electron Lett* 35:397–397
- Psaltis D, Quake SR, Yang C (2006) Developing optofluidic technology through the fusion of microfluidics and optics. *Nature* 442:381–386
- Rigler R, Elson ES (2001) *Fluorescence correlation spectroscopy*, 1st edn. Springer, Heidelberg
- Rindorf L, Jensen JB, Dufva M, Pedersen LH, Høiby PE, Bang O (2006) Photonic crystal fiber long-period gratings for biochemical sensing. *Opt Exp* 14:8224–8231
- Risk WP, Kim HC, Miller RD, Temkin H, Gangopadhyay S (2004) Optical waveguides with an aqueous core and a low-index nanoporous cladding. *Opt Exp* 12:6446–6455
- Russell P (2003) Photonic crystal fiber. *Science* 299:358–362
- Schelle B, Dreß P, Franke H, Klein KF, Slupek J (1999) Physical characterization of lightguide capillary cells. *J Phys D Appl Phys* 32:3157–3163
- Schmidt H, Yin D, Barber JP, Hawkins AR (2005) Hollow-core waveguides and 2D waveguide arrays for integrated optics of gases and liquids. *IEEE J Sel Top Quantum Electron* 11:519–527
- Schmidt O, Bassler M, Kiesel P, Johnson NM, Doehler G (2006) Guiding light in fluids. *Appl Phys Lett* 88:151109
- Smolka S, Barth M, Benson O (2007) Selectively coated photonic crystal fiber for highly sensitive fluorescence detection. *Appl Phys Lett* 90:111101
- Soref RA, Cortesi E, Namavar F, Friedman L (1991a) Vertically integrated SOI waveguides. *IEEE Photon Technol Lett* 3:19–21
- Soref RA, Schmidtchen J, Petermann K (1991b) Large single-mode rib waveguides in GeSi-Si and SOI. *IEEE J Quantum Electron* 27:1971–1974
- Squires TM, Quake SR (2005) Microfluidics: fluid physics at the nanoliter scale. *Rev Mod Phys* 77:977–1026
- Stryer L (1978) Fluorescence energy transfer as a spectroscopic ruler. *Annu Rev Biochem* 47:819
- Temelkuran B, Hart SD, Benoit G, Joannopoulos, Fink Y (2002) Wavelength-scalable hollow optical fibres with large photonic bandgaps for CO₂ laser transmission. *Nature* 420:650–653
- Tiefenthaler K, Lukosz W (1989) Sensitivity of grating couplers as integrated-optical chemical sensors. *J Opt Soc Am B* 6:209
- Uranus HP, Hoekstra HJWM, van Groesen E (2006) Considerations on material composition for low-loss hollow-core integrated optical waveguides. *Opt Commun* 260:577–582
- Vezenov DB, Mayers BT, Wolfe DB, Whitesides GM (2005) Integrated fluorescent light source for optofluidic applications. *Appl Phys Lett* 86:041104
- White IM, Suter JD, Oveys H, Fan X, Smith TL, Zhang J, Koch BJ, Haase MA (2007) Universal coupling between metal-clad waveguides and optical ring resonators. *Opt Exp* 15:646–651
- Whitesides GM (2006) The origins and future of microfluidics. *Nature* 442:368
- Winn JN, Fink J, Fan S, Joannopoulos JD (1998) Omnidirectional reflection from a one-dimensional photonic crystal. *Opt Lett* 23:1573
- Wolfe DB, Conroy RS, Garstecki P, Mayers BT, Fischbach MA, Paul KE, Prentiss M, Whitesides GM (2004) Dynamic control of liquid-core/liquid-cladding optical waveguides. *PNAS* 101:12434–12438
- Wolfe DB, Vezenov DV, Mayers BT, Whitesides GM, Conroy RS, Prentiss MG (2005) Diffusion-controlled optical elements for optofluidics. *Appl Phys Lett* 87:181105
- Xu Y, Lee RK, Yariv A (2000) Asymptotic analysis of Bragg fiber. *Opt Lett* 25:1756–1758
- Xu Q, Almeida VR, Panepucci RR, Lipson M (2004) Experimental demonstration of guiding and confining light in nanometer-size low-refractive-index material. *Opt Lett* 29:1626–1628
- Yan H, Gu C, Yang C, Liu J, Jin G, Zhang J, Hou L, Yao Y (2006) Hollow core photonic crystal fiber surface-enhanced Raman probe. *Appl Phys Lett* 89:204101
- Yeh P (2005) *Optical waves in layered media*, 2nd edn. Wiley, London
- Yeh P, Yariv A (1978) Bragg reflection waveguides. *Opt Comm* 19:427–430
- Yeh P, Yariv A, Hong C (1977) Electromagnetic propagation in periodic stratified media. I. General theory. *J Opt Soc Am* 67:423–438
- Yeh P, Yariv A, Marom E (1978) Theory of Bragg fiber. *J Opt Soc Am* 68:1196–1201
- Yin D, Barber JP, Hawkins AR, Deamer DW, Schmidt H (2004) Integrated optical waveguides with liquid cores. *Appl Phys Lett* 85:3477–3479
- Yin D, Barber JP, Hawkins AR, Schmidt H (2005a) Waveguide loss optimization in hollow-core ARROW waveguides. *Opt Exp* 13:9331–9336
- Yin D, Barber JP, Lunt EJ, Hawkins AR, Schmidt H (2005b) Optical characterization of arch-shaped ARROW waveguides with liquid cores. *Opt Exp* 13:10564–10569
- Yin D, Barber JP, Deamer DW, Hawkins AR, Schmidt H (2006a) Single-molecule detection sensitivity using planar integrated optics on a chip. *Opt Lett* 31:2136–2138
- Yin D, Barber JP, Hawkins AR, Schmidt H (2006b) Single molecule sensitivity and electrically controlled fluorescence detection in integrated planar ARROW waveguides. 2006 Conference on Lasers and Electro-optics (CLEO)
- Yin D, Lunt EJ, Barman A, Hawkins AR, Schmidt H (2007a) Microphotonic control of single molecule fluorescence correlation spectroscopy using planar optofluidics. *Opt Exp* 15:7290–7295
- Yin D, Lunt EJ, Rudenko MI, Deamer DW, Hawkins AR, Schmidt H (2007b) Planar optofluidic chip for single particle detection, manipulation, and analysis. *Lab Chip*. doi:10.1039/b708861b
- Zhang D, Lien V, Berdichevsky Y, Choi J, Lo Y (2003) Fluidic adaptive lens with high focal length tunability. *Appl Phys Lett* 82:3171–3172
- Zourob M, Mohr S, Treves Brown BJ, Fielden PR, McDonnell M, Goddard NJ (2003) The development of metal clad leaky waveguide sensor for the detection of particles. *Sens Actuators B* 90:296–307